Oil & Natural Gas Technology

DOE Award No.: DE-FE0001243

Topical Report

ATOMISTIC MODELING OF OIL SHALE KEROGENS AND ASPHALTENES ALONG WITH THEIR INTERACTIONS WITH THE INORGANIC MINERAL MATRIX

Submitted by:
University of Utah
Institute for Clean and Secure Energy
155 South 1452 East, Room 380
Salt Lake City, Utah 84112

Prepared for:
United States Department of Energy
National Energy Technology Laboratory

April 2011

Office of Fossil Energy

Atomistic Modeling of Oil Shale Kerogens and Asphaltenes along with their Interactions with the Inorganic Mineral Matrix

Topical Report

Reporting Period: October 1, 2009 – March 31, 2011

Authors: Julio C. Facelli, Ronald J. Pugmire, Ian S. Pimienta,

Shyam Badu, and Anita M. Orendt

Report Issued: April 2011

DOE Award No.: DE-FE0001243

Submitted by:
University of Utah
Institute for Clean and Secure Energy
155 South 1452 East, Room 380
Salt Lake City, UT 84112-0190

Prepared for:
United States Department of Energy
National Energy Technology Laboratory

Acknowledgement

This report was prepared as an account of work sponsored by an agency of the United States Government. Neither the United States Government nor any agency thereof, nor any of their employees, makes any warranty, express or implied, or assumes any legal liability or responsibility for the accuracy, completeness, or usefulness of any information, apparatus, product, or process disclosed, or represents that its use would not infringe privately owned rights. Reference herein to any specific commercial product, process, or service by trade name, trademark, manufacturer, or otherwise does not necessarily constitute or imply its endorsement, recommendation, or favoring by the United States Government or any agency thereof. The views and opinions of authors expressed herein do not necessarily state or reflect those of the United States Government or any agency thereof.

Abstract

The goal of this project is to obtain and validate three dimensional atomistic models for the organic matter in both oil shales and oil sands. In the case of oil shales the modeling was completed for kerogen, the insoluble portion of the organic matter; for oil sands it was for asphaltenes, a class of molecules found in crude oil. The three dimensional models discussed in this report were developed starting from existing literature two dimensional models. The models developed included one kerogen, based on experimental data on a kerogen isolated from a Green River oil shale, and a set of six representative asphaltenes.

Subsequently, the interactions between these organic models and an inorganic matrix was explored in order to gain insight into the chemical nature of this interaction, which could provide vital information in developing efficient methods to remove the organic material from inorganic mineral substrate. The inorganic substrate used to model the interaction was illite, an aluminum silicate oxide clay.

In order to obtain the feedback necessary to validate the models, it is necessary to be able to calculate different observable quantities and to show that these observables both reproduce the results of experimental measurements on actual samples as well as that the observables are sensitive to structural differences between models. The observables that were calculated using the models include ^{13}C NMR spectra, the IR vibrational spectra, and the atomic pair wise distribution function; these were chosen as they are among the methods for which both experimental and calculated values can be readily obtained. Where available, comparison was made to experiment results. Finally, molecular dynamic simulations of pyrolysis were completed on the models to gain an understanding into the nature of the decomposition of these materials when heated.

Table of Contents

List of Figures

List of Tables

I. Overview

The stated goals of this work are to obtain validated three dimensional (3D) models of kerogen, the insoluble organic matter found in sedimentary rocks such as oil shale, and asphaltenes, found in tar or oil sands. Asphaltenes, which are soluble organic fragments, can also be obtained from the breakdown or processing of kerogen. Subsequent to obtaining models, additional goals include modeling the interactions between these organic entities and an inorganic matrix in order to understand the chemical nature of this interaction, which could be vital information in developing new methods to remove the organic material from shale deposits using a much lower carbon footprint. The models are also used to calculate various observables such as spectroscopic data, which are then used to obtain feedback on the validity of the models by comparison of calculated observables to actual measurements on samples. These methods are also used to explore the sensitivity of the calculated observables to model details. Finally, the models are used to run simulations of the pyrolysis process under different processing assumptions.

There have been a number of different two dimensional (2D) models put forth for kerogens[1,2] as well as for asphaltenes.[3,4] The models are based on various experimental measurements. However, there is very little in the literature on 3D models.[1c,d] Obtaining validated 3D models is a crucial step in determining the structure of these materials, understanding the chemical nature of their interaction with the inorganic material, and calculating measurable properties of this matter. Understanding these interactions is critical to the development of novel strategies for efficiently separating the organic components from the inorganic matter.

The kerogen modeling work completed is based on Siskin's 2D model for a Type I kerogen from a Green River oil shale,[2] shown in Figure 1. Type I kerogens are those derived from marine organisms having hydrogen to carbon (H/C) ratios of greater than 1.25 and oxygen to carbon (O/C) ratios of less than 0.15. This model was constructed such that it can reproduce the elemental analysis, the experimentally determined distribution of functional groups, and the presence of structural features determined by various chemical treatments.

The work on asphaltenes was focused on the set of six 2D representative asphaltene structures reported by Siskin et al.[4] These 2D models were constructed using experimental data from solid state ^{13}C NMR, elemental analysis, and X-ray photoelectron spectroscopy. These six 2D structures are shown in Figure 2.

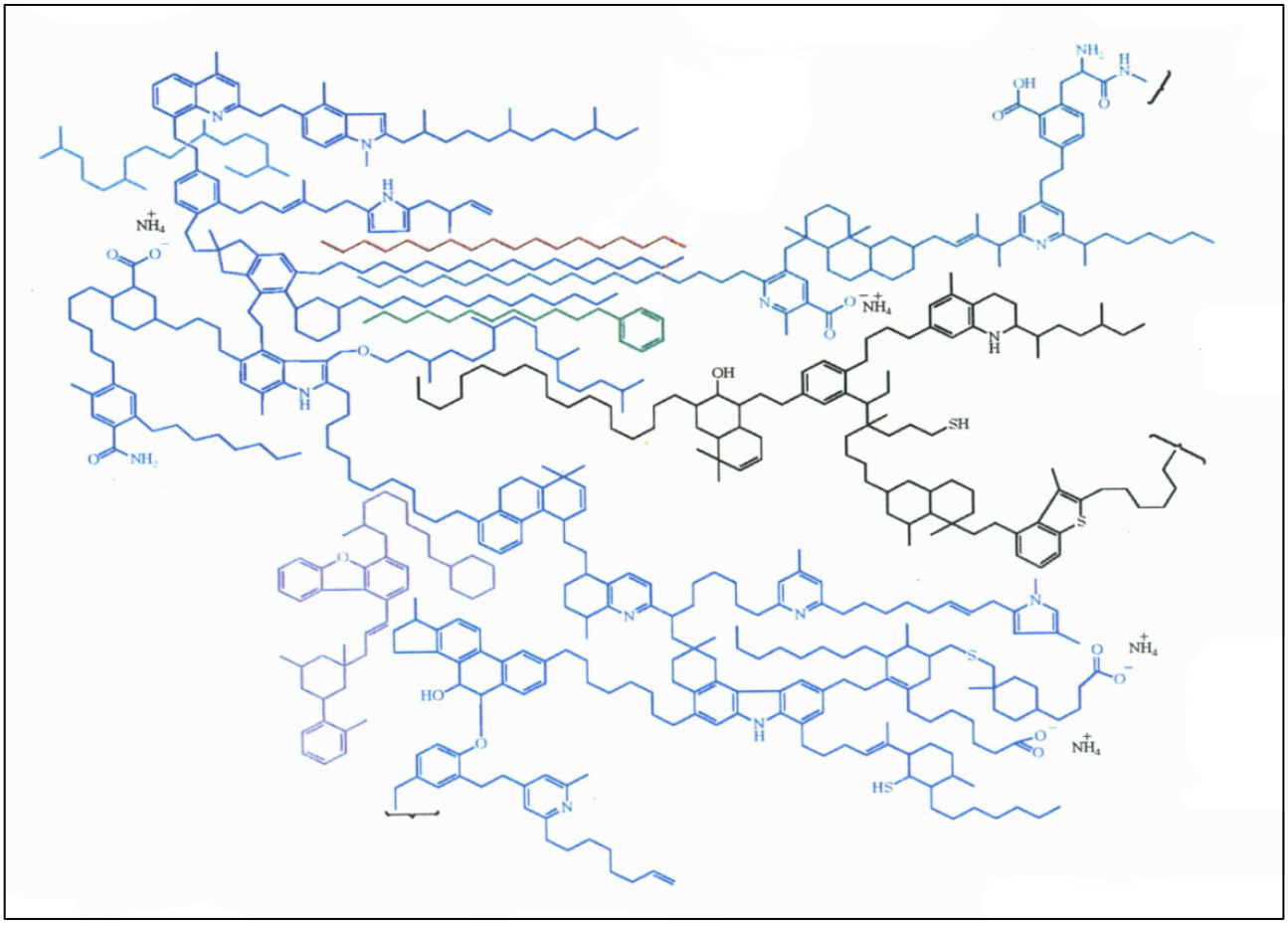

Figure 1: The 2D Siskin model of Green River kerogen. The model, composed of seven fragments, has a total molecular formula of $C_{647}H_{1017}N_{19}O_{17}S_4$ and a molecular weight of 9438.35 dalton. This model provided the chemical structure and the starting point for the 3D model developed in this project. From reference 2.

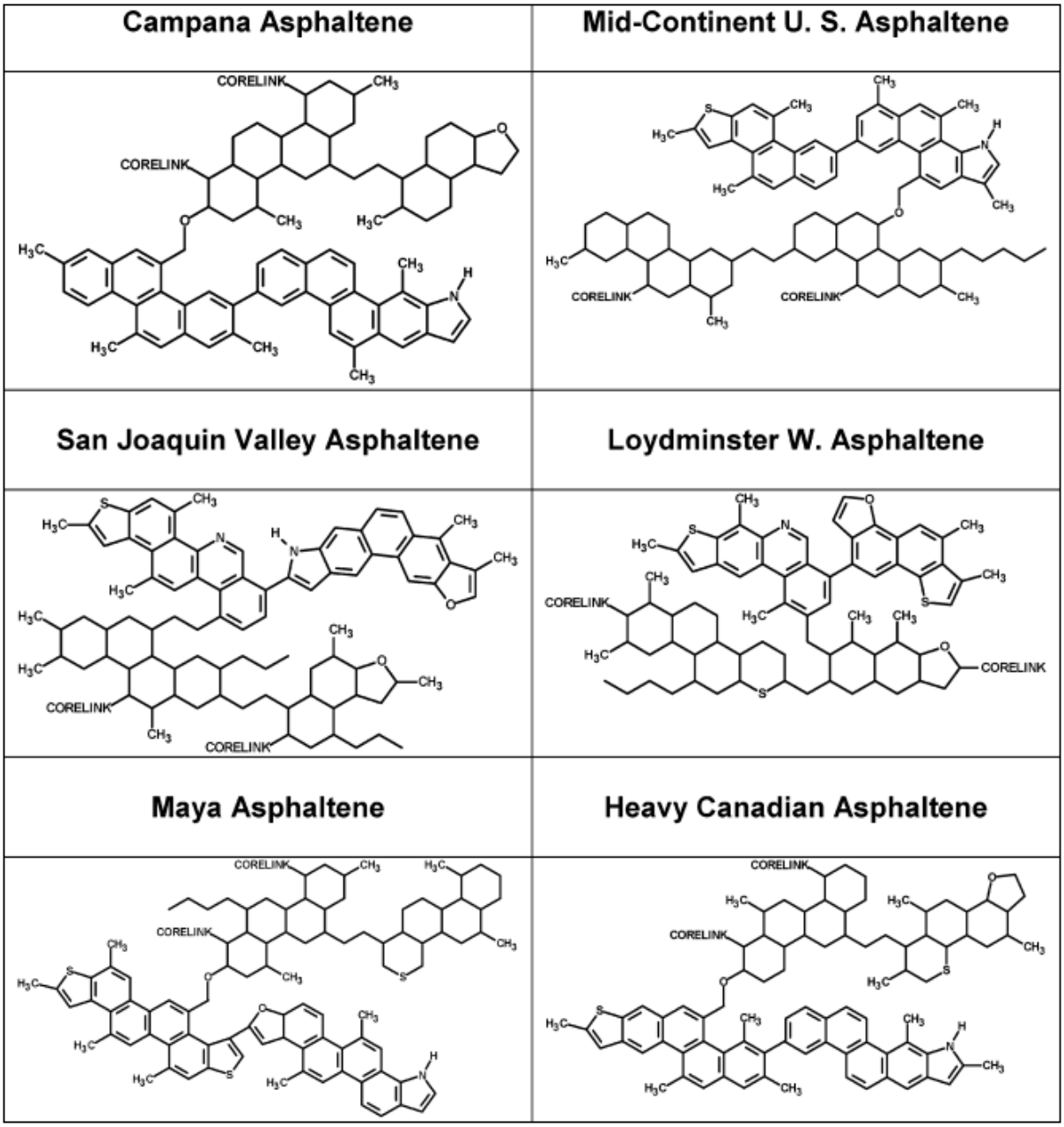

Figure 2: The six 2D structures of asphaltenes used as the starting point for the 3D models developed in this project. From reference 4.

Using the 3D models developed here, the ^{13}C NMR spectra, IR vibrational spectra, and the atomic pairwise distribution functions (PDF) were calculated. The models have also been used to run simulations of pyrolysis experiments.

II. *Computational Details*

All the computational work was done using computer resources available at the Center for High Performance Computing at the University of Utah. Programs used were HyperChem,[5] GAMESS,[6] Gaussian09,[7] ReaxFF[8] and DISCUS (part of the DIFFUSE[9] suite of programs). HyperChem was used for the molecular mechanic level calculations on the kerogen. ReaxFF, a reactive molecular dynamics package with an associated reactive forcefield, was used for the pyrolysis modeling. Both GAMESS and Gaussian09 were used for the ab initio level optimization calculations; Gaussian09 was also used for the calculation of the NMR and IR spectra with the final structures. DISCUS was used for the PDF simulations of the kerogen model structures.

III. Modeling of Kerogen

The modeling of the kerogen was done by molecular mechanics (MM), using the MM+ force field[10] as implemented in HyperChem to generate an initial 3D structure. This modeling was followed by further geometry optimizations at the ab inito level employing GAMESS for restricted Hartree Fock (RHF) calculations with a minimal STO-3G basis set. This starting 3D structure is shown in Figure 3.

This 3D STO-3G starting structure was subjected to a series of MM calculations using the simulated annealing procedure in Hyperchem to find better energies and to evaluate the diversity of possible structures within accessible energies at room temperature. The annealing involves heating the starting structure to a simulation temperature of 1200K, allowing it to evolve at this higher energy state for a set period of time, and then cooling it back to room temperature (300K). This process was repeated multiple times to generate a set of five new structures for our kerogen model. GAMESS was then used, again at the RHF/STO-3G level of theory, to perform geometry optimizations on each of these five structures. The lowest energy among these structures was then chosen as the new starting structure to repeat this process. This cycle of generating several structures via simulated annealing and geometry optimization to determine the lowest energy (most stable) structure was repeated four times, resulting in a decrease in the energy of the structure from -28569.2846 Hartree to -28571.4952 Hartree, a difference of 2.2106 Hartree or 1387 kcal/mol. These structures are presented in Figures 3 and 4 respectively.

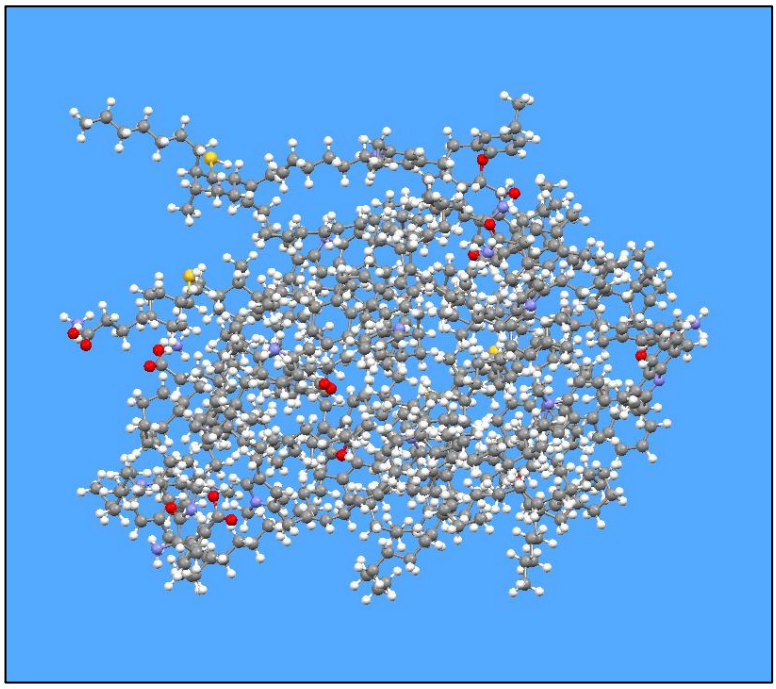

Figure 3: Initial 3D model of the Green River kerogen Siskin model (1702 atoms). The atom colors are: C - gray, O - red, N - blue, S - yellow, H - white. The tubes represent the molecule's backbone and the spheres represent the atoms. Total energy = -28569.2846 Hartree.

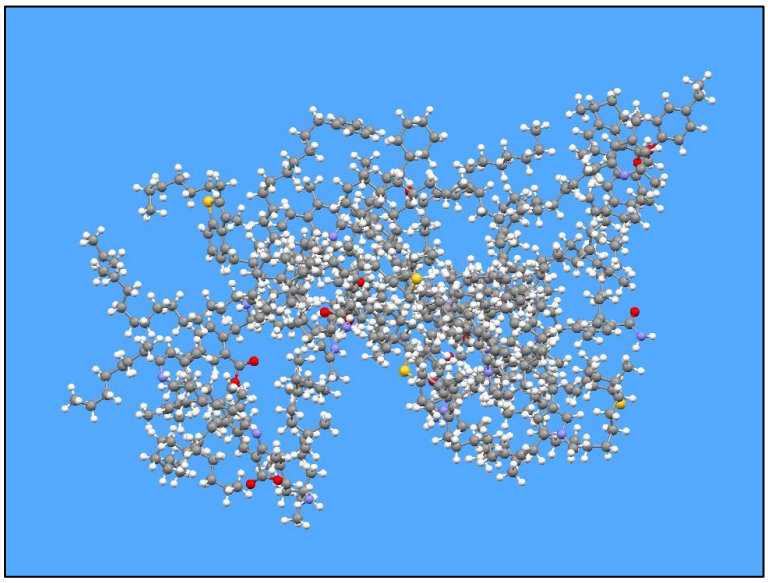

Figure 4: Lowest energy structure of kerogen model obtained by the four cycles of MM simulated annealing followed by ab initio geometry optimization. The atom colors and molecule description are the same as in Figure 3. Total energy = -28571.4952 Hartree.

This model, with 1702 atoms, is still considerably smaller than a "molecule" of kerogen and also had a much lower density. Hence, larger, higher density models were built by considering the structure in Figure 4 to be a monomer unit and using it to build larger models, including 2-, 3-, 4-, 5-, 6-, and 12-unit models. These larger models were needed to simulate the expected atomic pairwise distribution functions. Higher density was obtained by confining these models to a box and building the multi-unit structures to minimize any dead space. The 12-unit model, with a density of 0.90 g/ml, is shown in Figure 5. For comparison, an experimentally measured kerogen density is 0.95 g/ml .

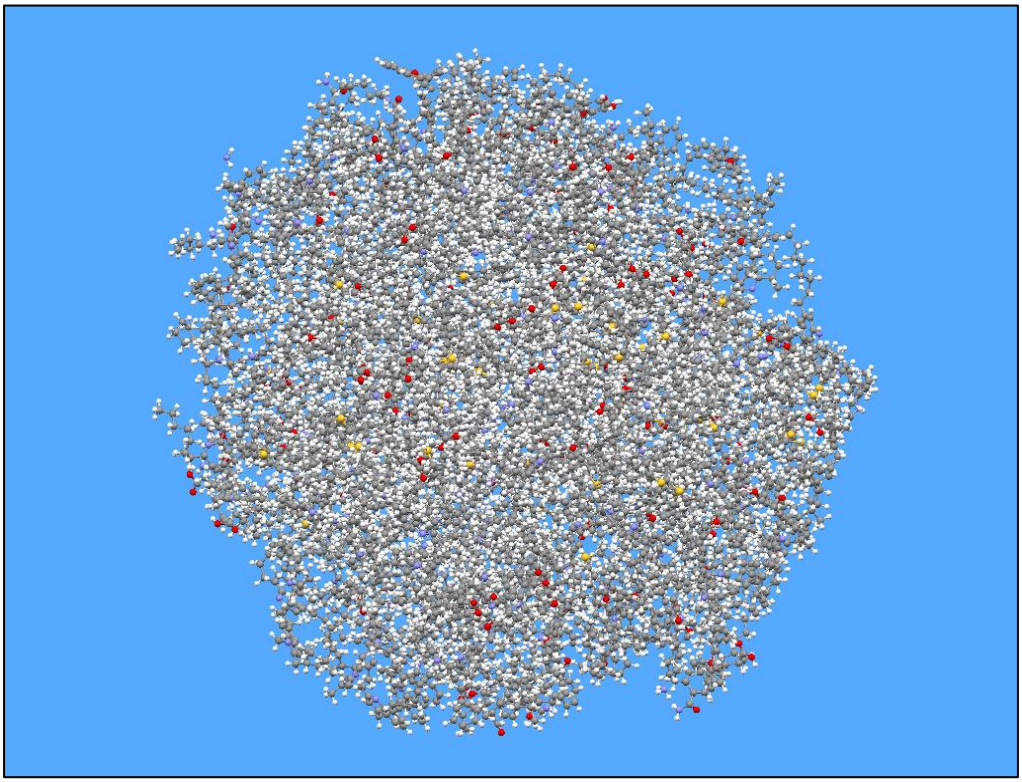

Figure 5: Three dimensional structure of 12-unit kerogen model (greater than 20,000 atoms). The atom colors and molecule description are the same as in Fig. 3.

IV: Modeling of Asphaltenes

The work done on the six asphaltene structures considered here included first building 3D models using HyperChem, followed by performing molecular mechanic level optimizations, and then using ab initio calculations (GAMESS, RHF with STO-3G basis sets) to further optimize the

structures. Attention was paid to the flexible bridging groups between the aromatic and aliphatic portions of the molecule present in each of the asphaltene structures as changes in this portion of the structure greatly affected the energy (stability) of the system. The rotation about these linkages was therefore explored to get the lowest energy structures, shown in Figure 6. These structures were then used to explore the aggregation of asphaltene units, which has been experimentally determined to occur,[11] to look at the interaction between the asphaltenes and a model inorganic matrix, and to predict the ^{13}C NMR and the IR spectra of the different models.

It has been reported that these asphaltene units tend to aggregate as stacks as a result of intermolecular forces between the units;[11c] therefore, calculations to determine the preferred stacking orientation were performed in one of the asphaltenes (Campana model). The calculations to study the packing were first done on stacks of three Campana units using Gaussian09 at the Density Functional Theory (DFT) level using the new M06-2X functional[12] that was developed for the study of non-bonding interactions and the MIDI basis set. Three different stacking patterns were studied: i) parallel or stacked one above each other, ii) anti-parallel or stacked above each other but rotated 180° about the major plane of the asphaltene, and iii) inverted or stacked above each other and rotated 180° about the other axis of the unit. The parallel stack was found to be the lowest in energy; this makes sense at it is the orientation that allows for the closest packing.

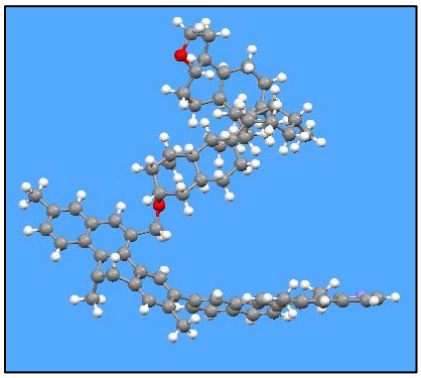

Campana

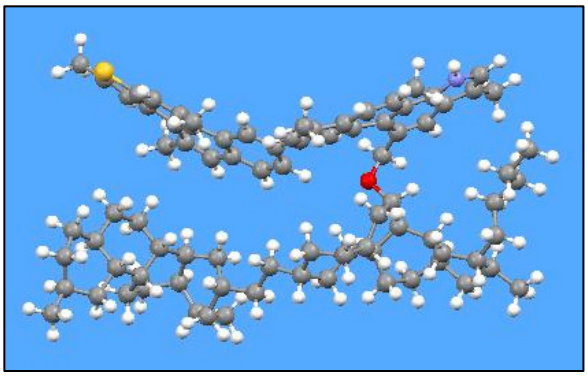

Mid-Continent US

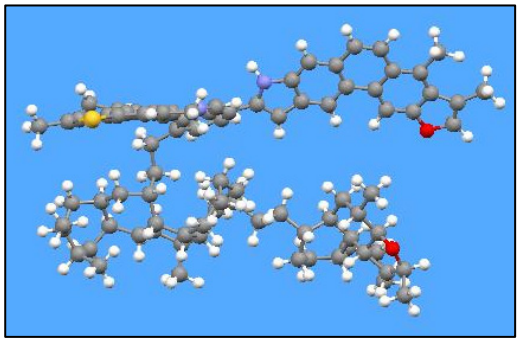

San Joaquin Valley

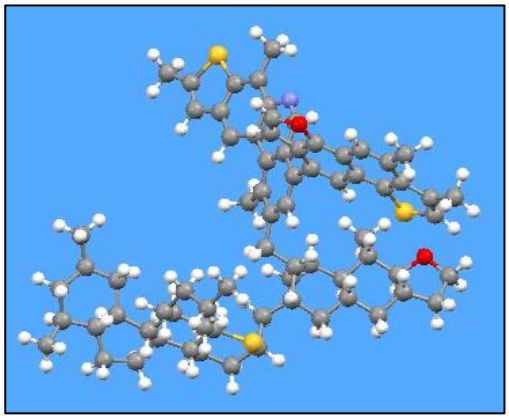

Loydminster Wainwright

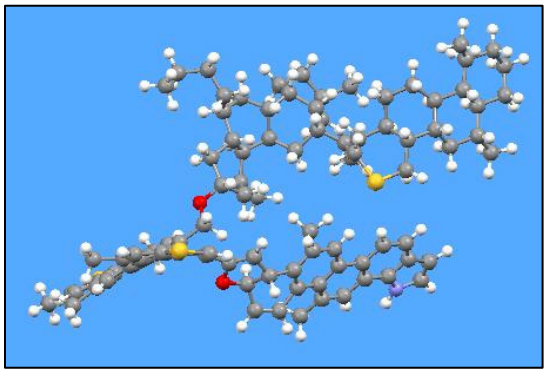

Maya

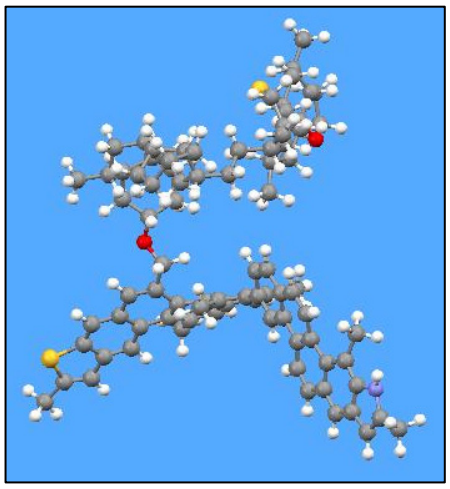

Heavy Canadian

Figure 6: Three dimensional models of asphaltenes. The atom colors are: C - gray, O - red, N - blue, S - yellow, H – white

The lowest energy structure for each of these stacking patterns is shown in Figure 7; their relative energy is given in Table 1. These energies can be compared to the energy of three single Campana units which is -9750.2691 Hartree, i.e., three times the energy calculated for a single unit optimized at the same level of theory (-3250.0897 Hartree). As this is a lower energy than any of the stacks, these calculations do not support the experimental observation that aggregation occurs due to intermolecular interactions stabilizing the structure. Note that the Basis Set Superposition Error (BSSE)[13], while not considered here, will lead to an even lower energy for the non-interacting configurations. Further calculations exploring other models, other levels of theory, and/or stacking arrangements must still be completed.

Table 1: Energies of Campana asphaltene stacks

Asphaltene Stack	Total Energy (Hartree)	Relative Energy (kcal/mol)
Parallel	-9750.2572	0
Anti-parallel	-9750.2334	+14.9
Inverted	-9750.2235	+21.1

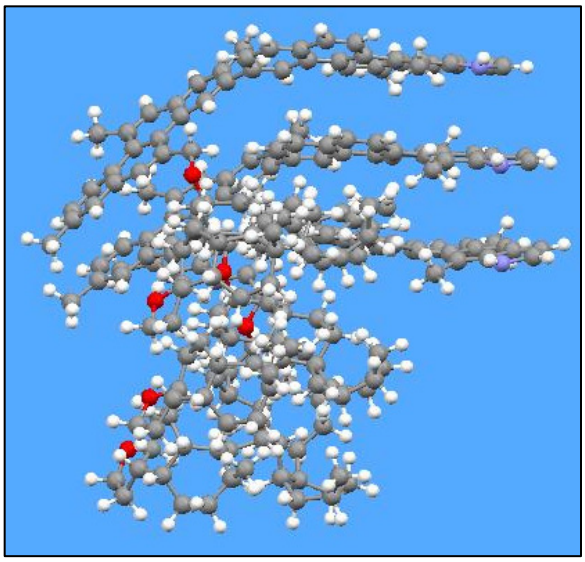

Parallel

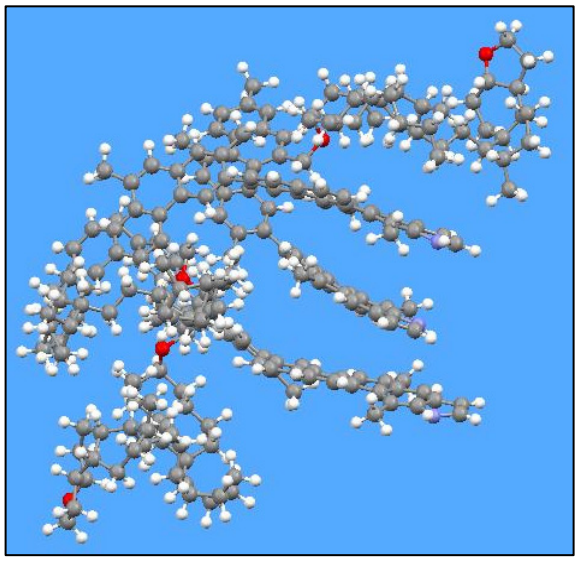

Inverted

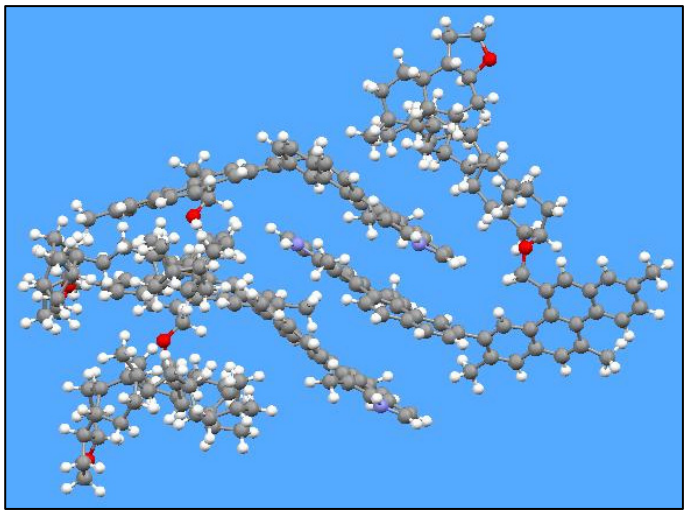

Anti-parallel

Figure 7: Lowest energy structures for the three types of stacking studied for the Campana asphaltene.

V: Interaction with the Inorganic Matrix

The interaction of the six asphaltene model structures discussed above with an inorganic illite matrix (aluminum silicate oxide clay) structure[14] was studied at two different levels of theory using Gaussian09. An example structure for the asphaltene illite is shown in Figure 8.

The calculations of the interaction between all six asphaltene structures and the illite matrix were completed at the molecular mechanics level of theory using the Universal force field

(UFF),[15] starting with the structures described above for the six different asphaltenes. The change in the interaction energy as a function of the separation between the asphaltene and the illite was studied, without allowing the structures of the illite or asphaltene to change. The largest binding energies between the asphaltene and the illite, corresponding to the separation with the minimum total energy, are reported in Table 2. These calculations were followed by single–point PM6 semi-empirical calculations at the separation with the minimum UFF energy; these binding energies are given in the last column of the table. Negative binding energies, given in the last two columns, indicate that there is no binding between the asphaltene and the illite, at least in the current calculations.

Table 2: Energy of interaction between the asphaltene and the illite[a]

	Asphaltene alone (kcal/mol)	Illite alone (kcal/mol)	Sum of isolated Asphaltene and Illite (kcal/mol)	Asphaltene and illite at minimum E separation (kcal/mol)	UFF Binding Energy (eV)	PM6 Binding Energy (eV)
Campana	442.22	50464.45	52131.64	50906.67	-53.12	-0.88
Heavy Canadian	409.06	50464.45	52096.53	50873.51	-53.04	-0.13
Loydminster W.	320.21	50464.45	50762.53	50784.67	0.96	-1.10
Mid-Continent US	385.42	50464.45	51430.84	50849.87	-25.19	-8.14
Maya	473.65	50464.45	52056.76	50938.10	-48.51	-0.82
San Joaquin Valley	431.69	50464.45	50849.53	50896.15	2.02	-1.38

[a]All energies except for the last column refer to the calculations at the UFF level.

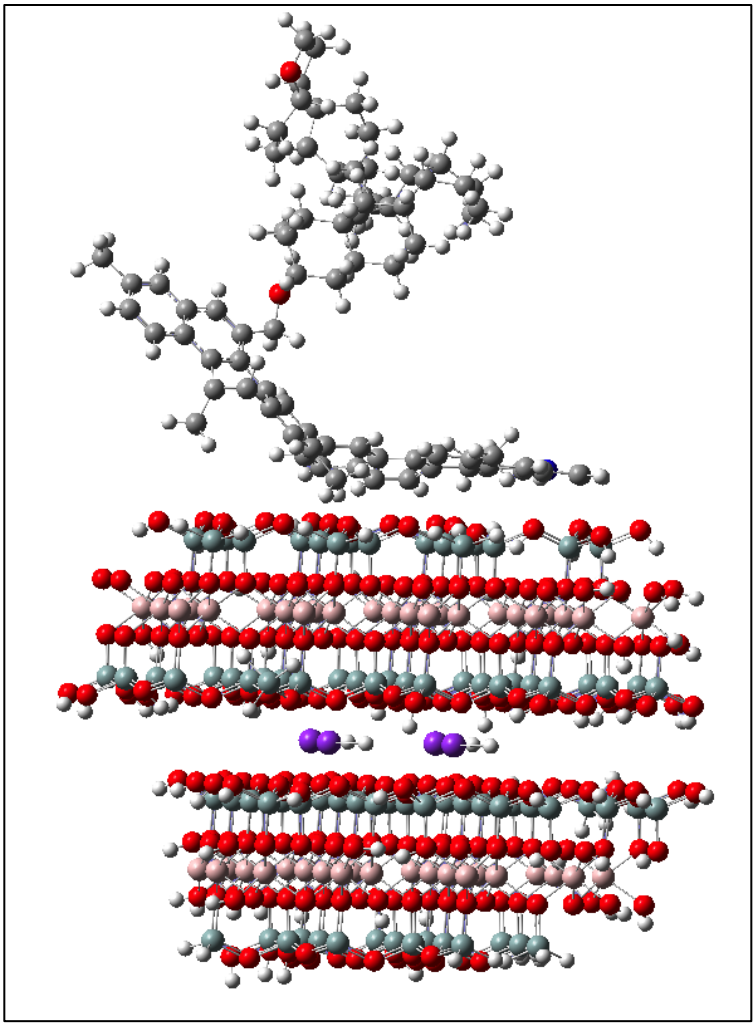

Figure 8: Model of interaction between Campana asphaltene and Illite. The atom colors in the asphaltene are: C - gray, O - red, N - blue, H – white; in the illite they are: Si – gray, O – red, H – white, Al – pink, and K – purple.

VI: Calculation of Spectroscopic Data and Comparison to Experimental Results

One way to validate the model structures is to assess if molecular properties calculated with the model reproduce the results of experimental measurements on the materials of interest. The choice of molecular properties or observables that were chosen to be used was a function of the reliability of the calculations to be able to accurately reproduce experimental measurements, of the sensitivity of the observable to the 3D structure of the model, and on the ability to be able to obtain experimental measurements of the observable on kerogen and asphaltene samples.

There exist theories that can be readily used to calculate both IR frequencies and NMR chemical shifts, and they have been incorporated into many available software packages, including Gaussian and GAMESS; the use of these calculations to understand and/or interpret atomic level structure is routine. In addition, these are experimental techniques that are readily available at the University of Utah and relatively easy to obtain on oil shale and oil sands samples, on isolated kerogen and asphaltene, and on the products of pyrolysis experiments. NMR chemical shift and IR frequencies are both sensitive to details about the chemical environment such as functional groups present and neighboring atoms as well as to information on intra- and inter-molecular interactions.

Small angle X-ray scattering (SAXS) can provide structural information at length scales ranging from the angstrom to micrometer sizes, including information on particle shape and size, particle size distribution, and pore size and distribution. Pairwise Distribution Functions (PDF) measurements provide a plot of the structural information from the sample as a function of the frequency of interatomic distances. Using available software, SAXS scattering curves and the expected PDF profiles for the various models can be computed. In case of the PDF measurement, this can be done using the DISCUS program available in the DIFFUSE package.[9] For SAXS, the programs CRYSLOL[16] or ORNL_SAS[17] are available to predict the scattering curves given the atomic coordinates of the system. Both measurements can be accomplished at the user facility at the Advanced Photon Source at Argonne National Laboratory.

^{13}C NMR Spectra: The NMR calculations were done with the Gaussian09 program using the PBE1PBE DFT functional and the 6-311G basis function on the minimum energy structures of the six asphaltenes discussed above. The resultant ^{13}C chemical shielding values were referenced to the TMS scale with the chemical shielding of CH_4 at the same level of theory and the basis set being referenced to the known gas phase chemical shift of CH_4 of -7 ppm.[18] The calculated chemical shifts were then broadened (aliphatic with 2.5ppm, aromatic with 5ppm) and plotted.

The plots of the spectra of all six of the asphaltenes are shown in Figure 9. The six spectra show very distinct features, indicative of how sensitive NMR chemical shifts are to the differences in the structural features of the models. In Figure 10 the calculated spectrum of the Mid-Continent asphaltene is compared with the corresponding experimental solid state ^{13}C spectrum; this is the only asphaltene for which the experimental ^{13}C NMR spectrum has been published.[4] However, from the analysis of the spectra presented in Siskin and Kelemen's *Energy & Fuels* paper,[4] it is expected that the six spectra will show marked differences. For example, the analysis presented in the paper states that three of the asphaltenes (Mid-Continent US, San Joaquin Valley, and Loydminster Wainwright) have 35-40% aromatic carbons (chemical shifts between 90 and 165 ppm), whereas the other three (Campana, Maya, and

Heavy Canadian) have 45-50% aromatic carbons. Further analysis shows that the breakdown of all aromatic carbons to those that are either protonated, bridgehead, or substituted by carbon also varies greatly between the asphaltenes from the six different locations.

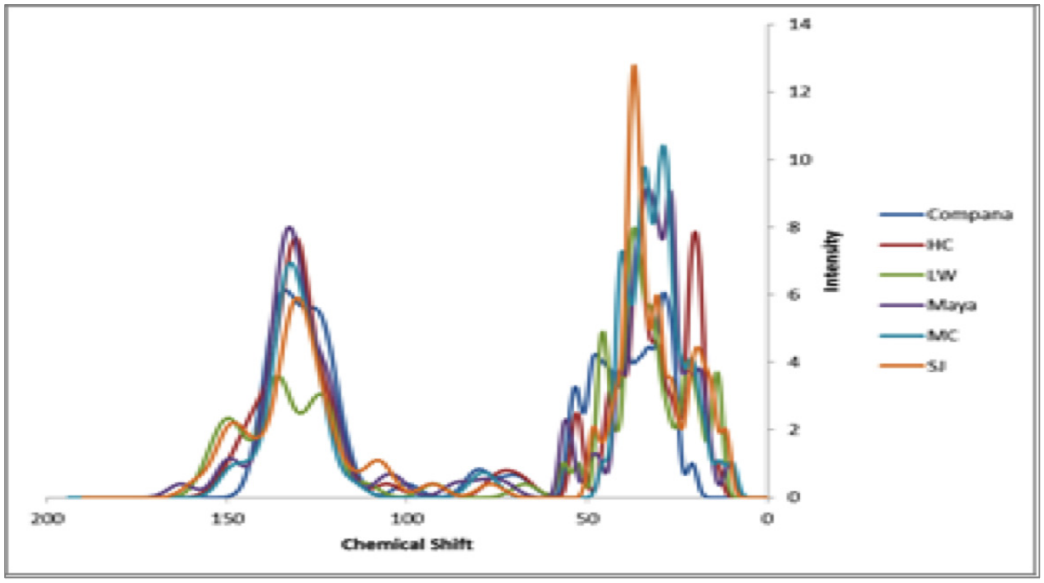

Figure 9: Comparison of calculated ^{13}C NMR for the six different asphaltene models.

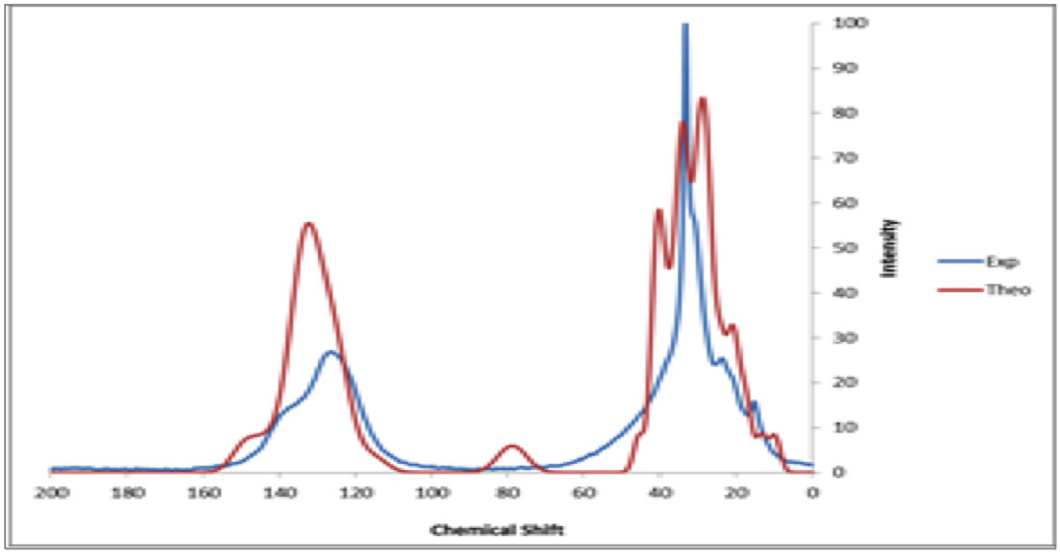

Figure 10: Comparison of calculated and experimental ^{13}C NMR of mid-continent US asphaltene.

As mentioned earlier, asphaltenes are known to aggregate via stacking, and intermolecular interactions can contribute to observed chemical shifts. Previously, optimized stacks of three of the Campana asphaltenes in three different manners were obtained. The parallel stack was determined to be the lowest energy of these three and therefore this stack was used for the chemical shielding calculations. Figure 11 shows the comparison of the calculated ^{13}C NMR chemical shifts for the single Campana unit and the parallel stack.

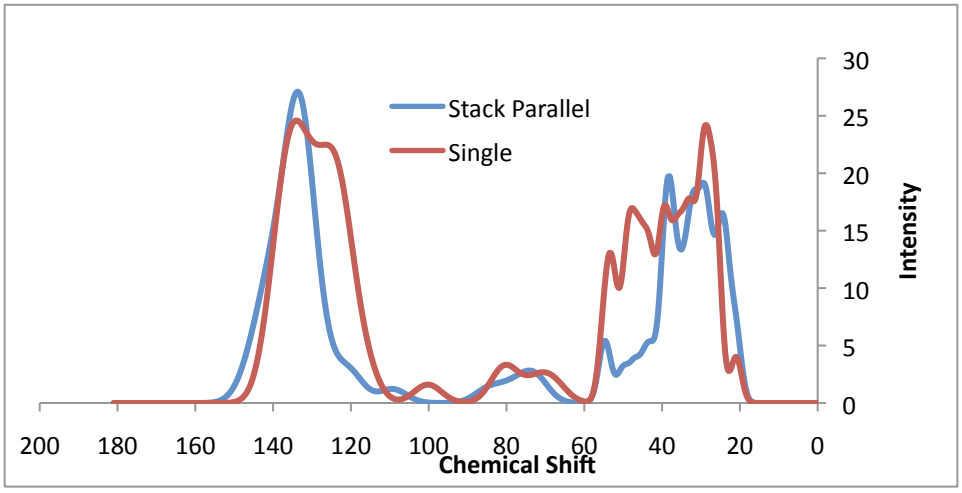

Figure 11: Comparison of calculated ^{13}C NMR of single unit and the parallel stack (lowest E stack) for model of Campana asphaltene.

The same NMR calculations were completed at the STO-3G basis set for the single unit kerogen structure reported above; this spectrum is shown in Figure 12.

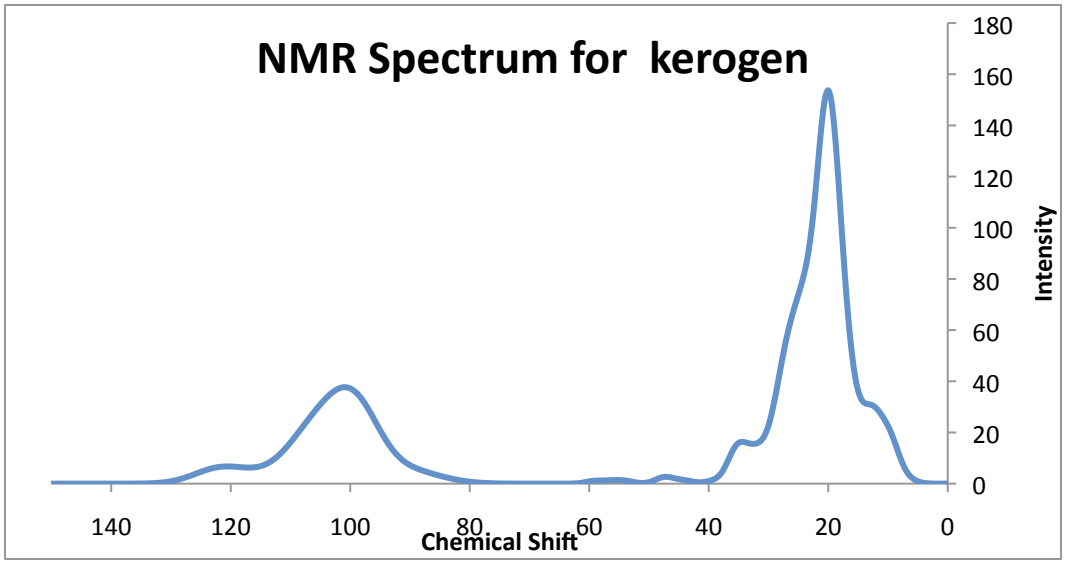

Figure 12: Calculated ^{13}C NMR spectrum for kerogen based on single unit of kerogen model.

This calculated ^{13}C NMR spectrum of kerogen can be compared to the preliminary experimental ^{13}C NMR spectrum obtained on the kerogen isolated from a section of the Skyline 16 core, shown in Figure 13. The kerogen was isolated from the section of peak organic content in the Mahogany zone.

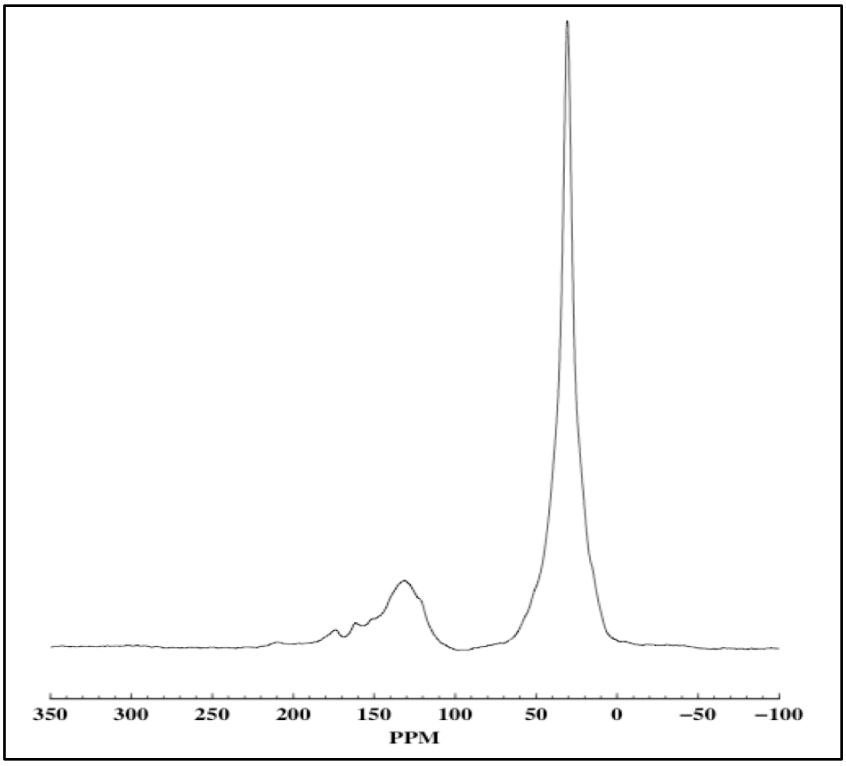

Figure 13: Experimental ^{13}C NMR spectrum from Skyline 16 core sample in Mahogany zone at depth of 462-463 feet.

IR Vibrational Spectra: The vibrational frequencies, measured in wavenumber with the unit of cm^{-1}, for the six different single molecule asphaltene models were also calculated and used to provide simulations of the expected experimental IR spectra. The exact vibrational frequencies observed depend on a complex relationship involving the strength of the bonding between atoms, the symmetry of the system and the chemical environment about the involved atoms; each vibrational frequency (there are 3N-6 fundamental vibrational frequencies for a molecule, where N is the number of atoms in the system) involves a complex stretching and bending of groups of atoms. For example, C-H stretches are observed in the range of 2850 to 3100 cm^{-1}; only if there are protonated alkene or aromatic carbons will stretches be observed above 3000 cm^{-1}.

These calculations were completed on the same STO-3G optimized structures with Gaussian09 using the same functional mentioned above but at the smaller STO-3G basis set level. The choice of a smaller basis set was dictated by the requirement that vibrational frequencies can only be calculated on completely optimized geometries. The resulting calculated IR spectra are shown in Figure 14 for two of the six asphaltenes. As can be seen from these spectra, IR is a

second spectroscopic method that is sensitive to changes in the model structure and that can be used for validation of the models, as such experimental data becomes available.

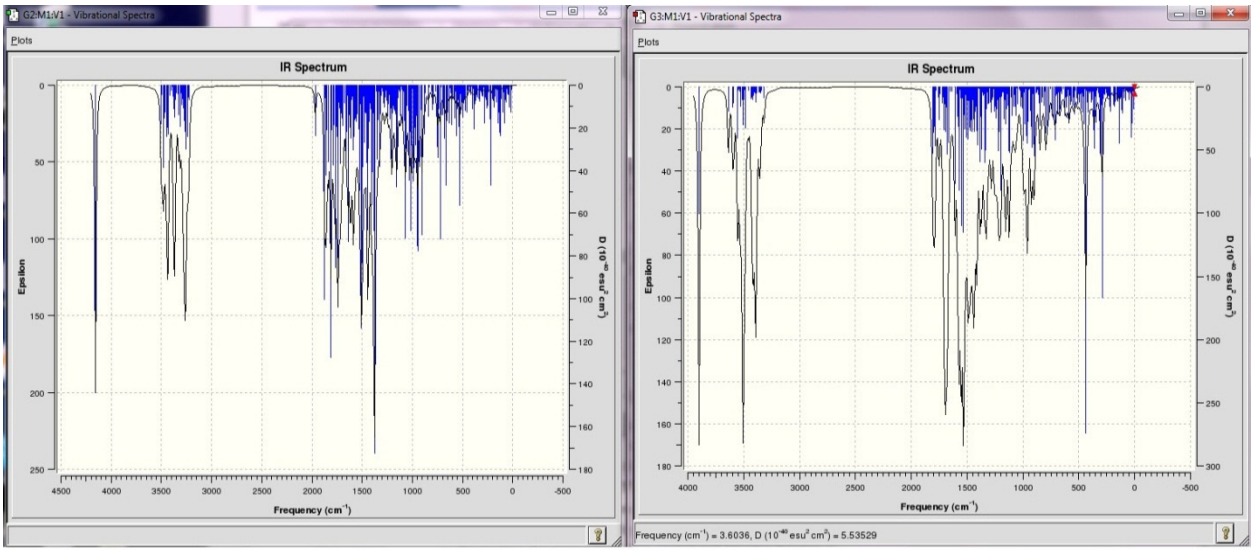

Figure 14: Calculated IR spectra of two model asphaltenes: Campana (right) and Mid-continent US (left)

PDF: PDF measurements provide a plot of the structural information from the sample as a function of the frequency of interatomic distances. At the short range, the distances correlate with the bond lengths or the separation of directly bonded atoms, but as the atomic separation increases, the distances are a reflection of the dihedral angles in the sample. As with NMR and IR spectra, simulations of the PDF profile expected for a given structural model can be completed in order to evaluate the models. The calculation of the PDFs based on our 3D kerogen models were completed using the DISCUS program. The resulting plots are shown in Figure 15. The peaks at the small distances (labeled "Radius" in the figure) are consistent with known C-H and C-C bond lengths and expected three atom separations for C-C-H and C-C-C entities. The features at longer separations are due to four atom separations (defined by dihedral angles) and other longer range separations – features that are very dependent on the 3D structure.

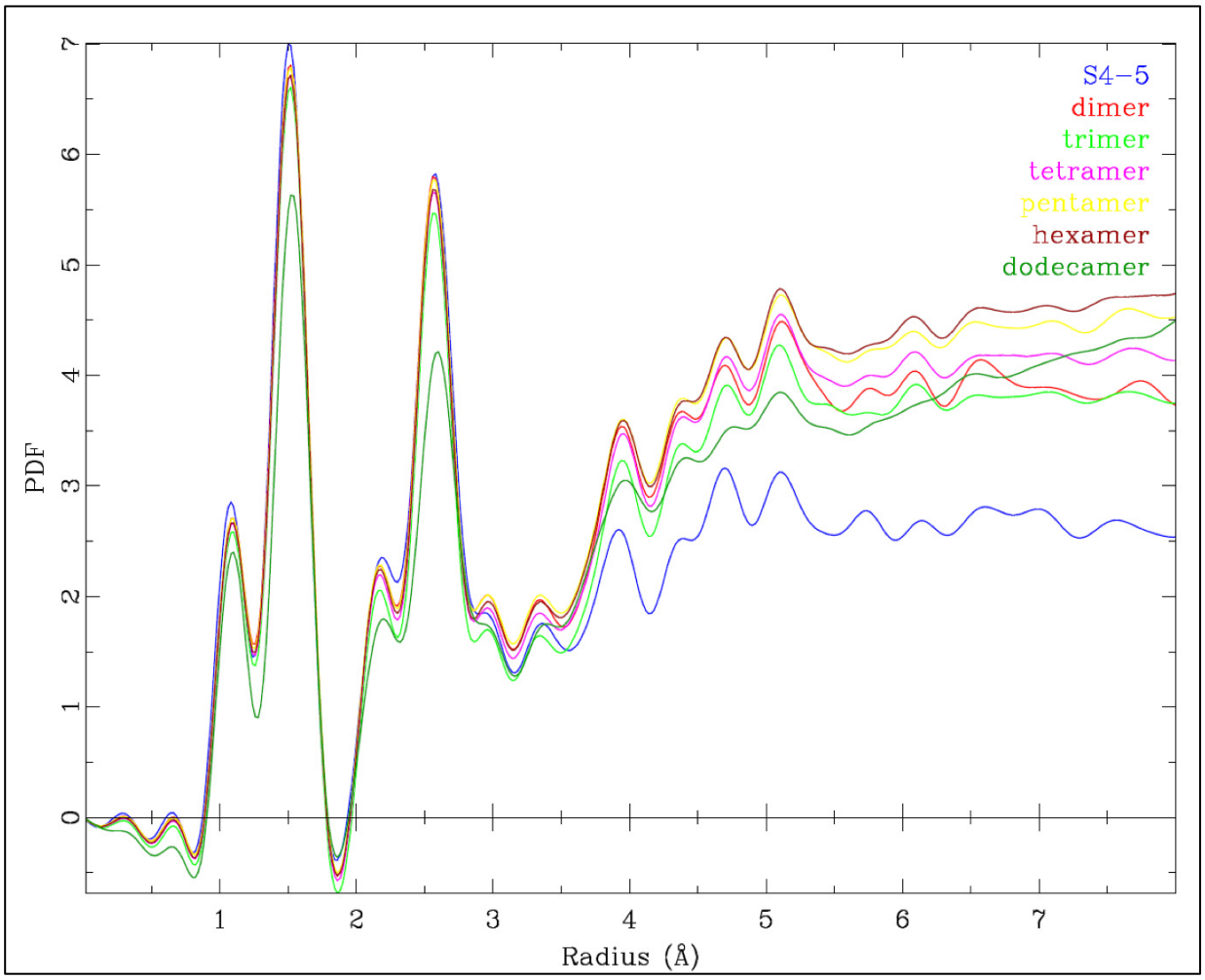

Figure 15: Calculated PDF showing the interatomic distance distribution for the different sized kerogen models.

VII: Pyrolysis modeling

Pyrolysis is a thermochemical decomposition of organic materials at elevated temperature in the absence of oxygen. To analyze the pyrolysis products of asphaltenes, the Reactive Force Field reactive molecular dynamics (ReaxFF MD) simulation was used.[8] The ReaxFF force field is a bond order dependent force field that provides accurate descriptions of bond breaking and bond formations, based on the calculation of the bond orders from interatomic distances at each step of the molecular dynamics simulation. In this force field the valence interactions (bond angle, torsion) and charge are allowed to change continuously as bonds form and break in the reaction. The energy function for ReaxFF has the following form:

$$E_{system} = E_{bond} + E_{over} + E_{under} + E_{val} + E_{pen} + E_{tor} + E_{conj} + E_{vdw} + E_{coloumb}$$

In the expression above, E_{bond} denotes the bond energy, E_{over} and E_{under} are the over- and under-coordinated atom in the energy contribution and E_{val}, E_{pen}, E_{tors}, E_{conj}, E_{vdw}, and $E_{coulomb}$ are the valence angle term, penalty energy, torsion energy, conjugation effects to molecular energy, nonbonded van der Waals interaction and Coulomb interaction, respectively.[8] When the ReaxFF MD simulation is performed, the reactions that can occur include the cleavage of C-C, C-O and C-N bonds to form smaller hydrocarbons, dehydrogenation to form two radicals (H and remainder of molecule), and hydrogen abstraction.

The ReaxFF MD technique has been used to study reactivity (decomposition, combustion, pyrolysis, chemisorption) in a wide range of systems including polymers,[19] explosives,[20] jet fuel,[21] and nanoparticles.[22] Most relative to the pyrolysis of the kerogen and asphaltenes are two papers dealing with the pyrolysis of an aliphatic fossil organic biopolymer[23] and the maturation process in a Morwell Brown coal.[24] With this literature in mind, this technique was applied to the asphaltene systems.

A molecular dynamics (MD-NVT) simulation was first completed on a single asphaltene unit, starting with the ab initio optimized structures discussed above. In an MD-NVT simulation, also known as a constant temperature simulation, the number of atoms [N], the volume [V], and the temperature [T] are kept constant. During the simulation, the energy of the exothermic and endothermic processes is exchanged with a thermostat such as the Nose-Hoover thermostat,[25] the Berendsen thermostat[26] and the Langevin thermostat.[27] In these simulations, the Berendsen thermostat was used. The box volume used for the simulations was 28×18×32 $Å^3$; temperatures ranged from 1000K and 3000K. The simulations were allowed to run for 50 picoseconds (ps). Because the simulation time in these types of simulations is many orders of magnitude less than the times of experimental pyrolyses, the temperature used is much higher than the actual experimental temperatures. However, even with these differences in the time and temperature scale, the simulations have been shown to provide qualitative agreement with experimental products.[23]

Figure 16 shows the results of the ReaxFF MD-NVT simulation, in terms of the number of fragments versus the simulation time, for the pyrolysis of a single Campana asphaltene unit at different temperatures. While the simulation was run starting from temperatures of 1000K, it was found that for the timescale studied here, the decomposition of the molecule starts at 2000K. Therefore, Figure 16 presents the number of fragments obtained at the constant temperatures of 2000K and above. From the figure it is clear that the trend is to produce more fragments as the temperature is increased, as is expected. It should be noted that the pyrolysis is a very dynamic process, with some bonds being broken and others forming over time.

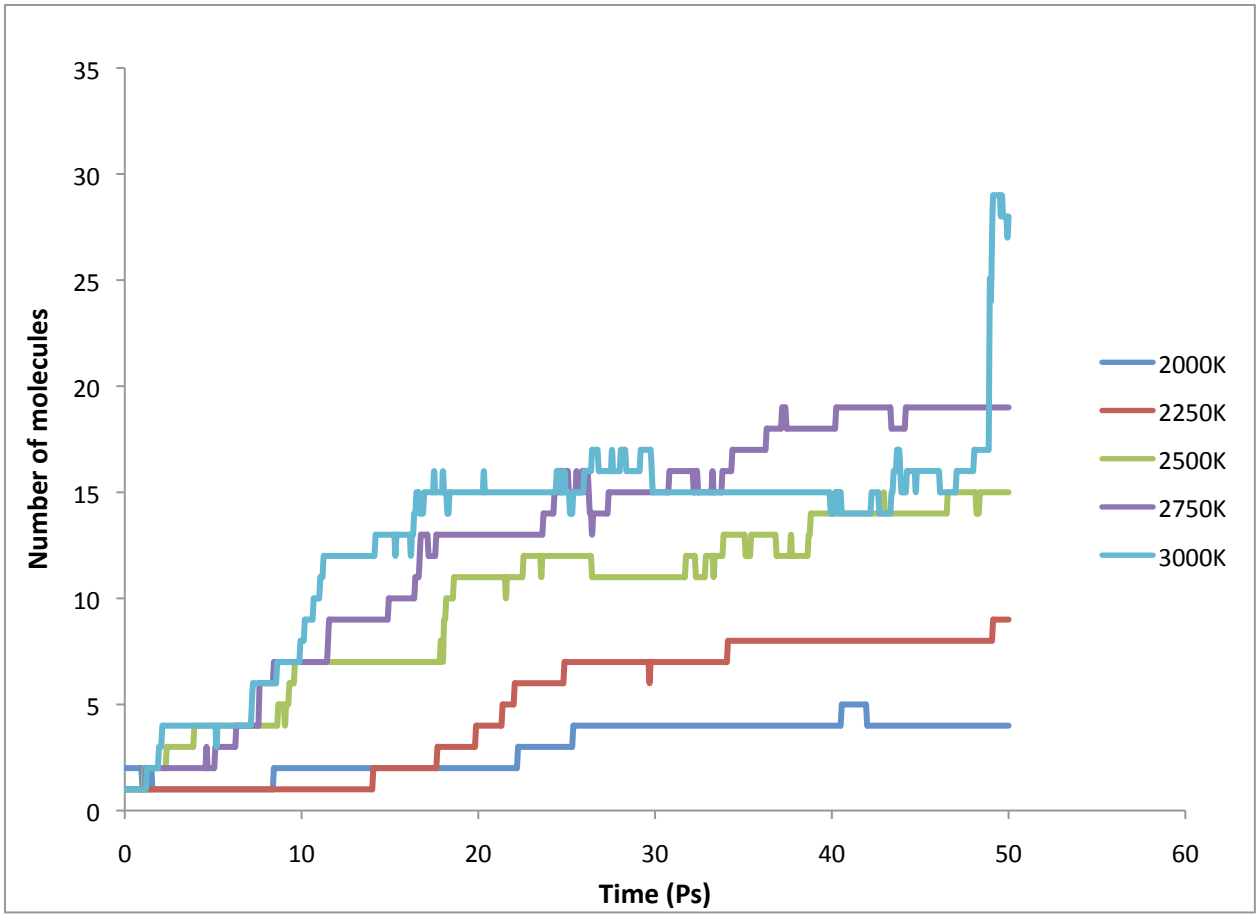

Figure 16: Results of NVT-MD simulation of a single Campana asphaltene unit at different temperatures.

The same MD-NVT simulation was also performed on the different stacks of three Campana asphaltene units, again starting from the ab initio optimized structures. The box size taken for the parallel stack was 41×33×36 $Å^3$, for the anti-parallel stack was 53×35×28 $Å^3$, and for the inverted stack was 56×30×30 $Å^3$. The same plots for the number of fragments as a function of the simulation time results at different temperatures for these three stacks are presented in Figures 17, 18, and 19. The results for these three stacks of asphaltene show a similar trend to the single Campana asphaltene unit: an increasing number of product molecules with increasing temperature.

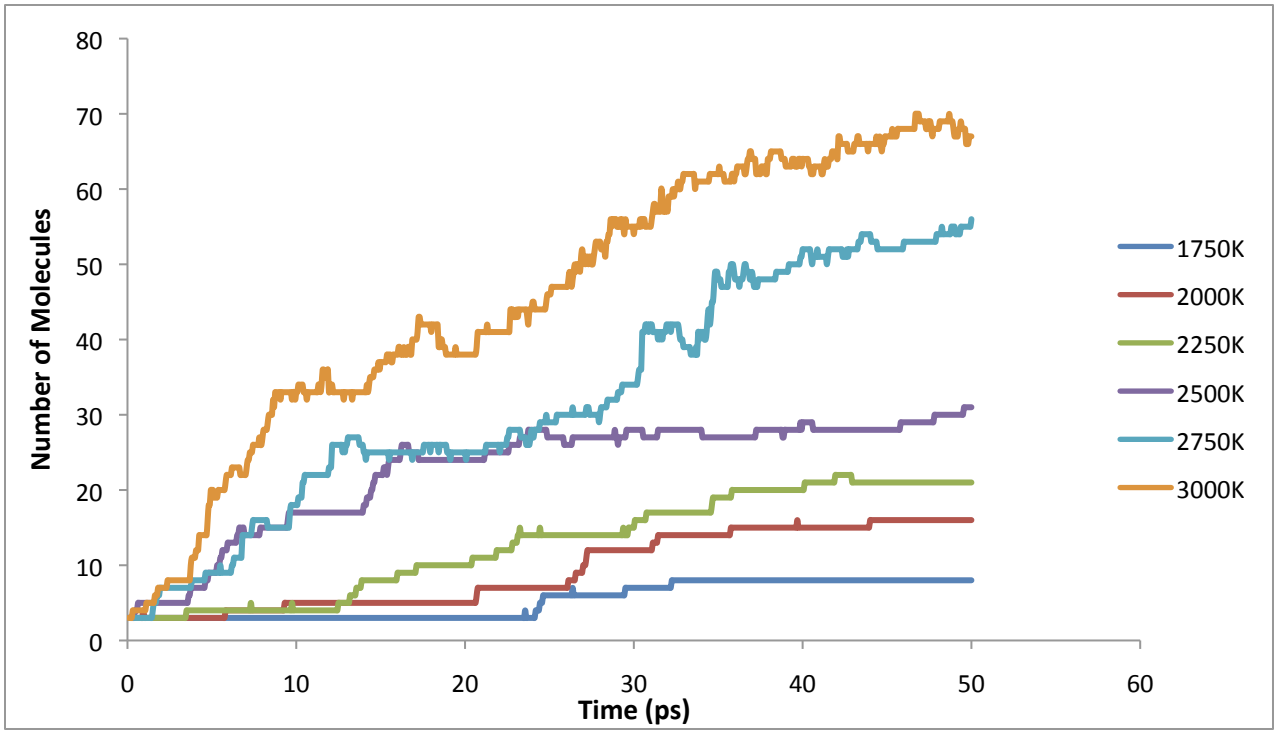

Figure 17: Results of NVT-MD simulation of parallel stack of three Campana asphaltene units at different temperatures.

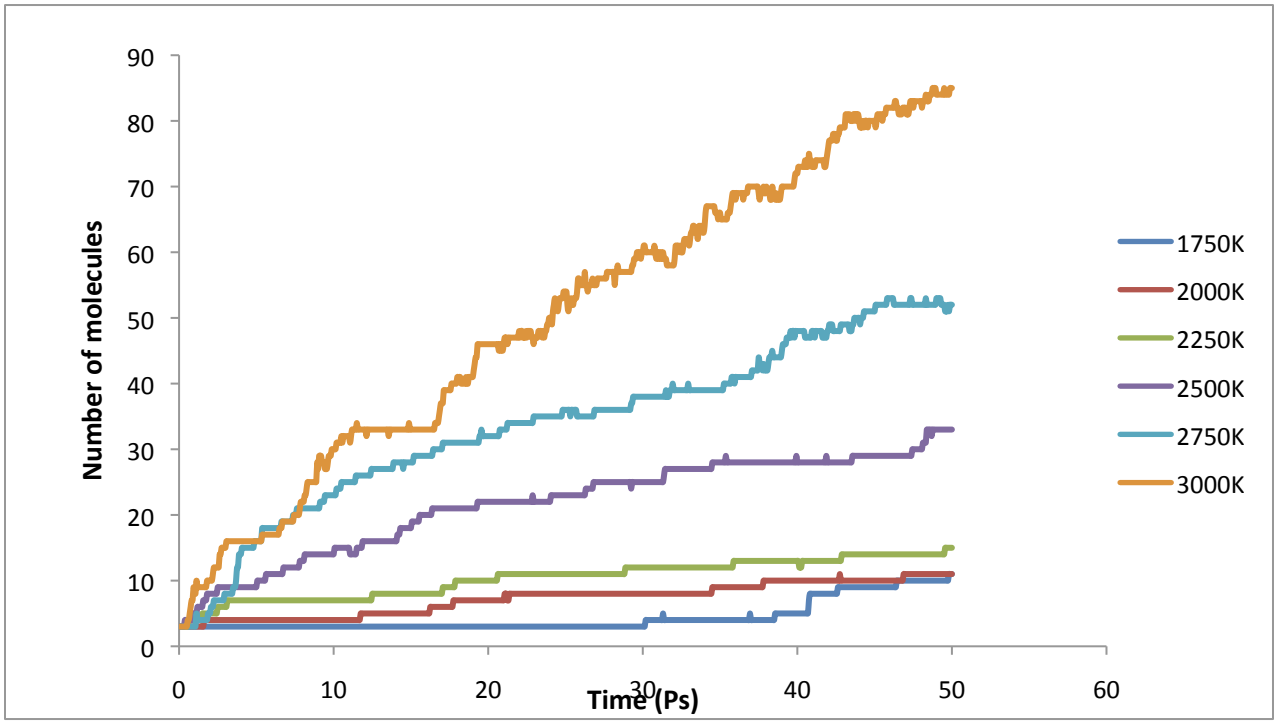

Figure 18: Results of NVT-MD simulation of anti-parallel stack of three Campana asphaltene units at different temperatures.

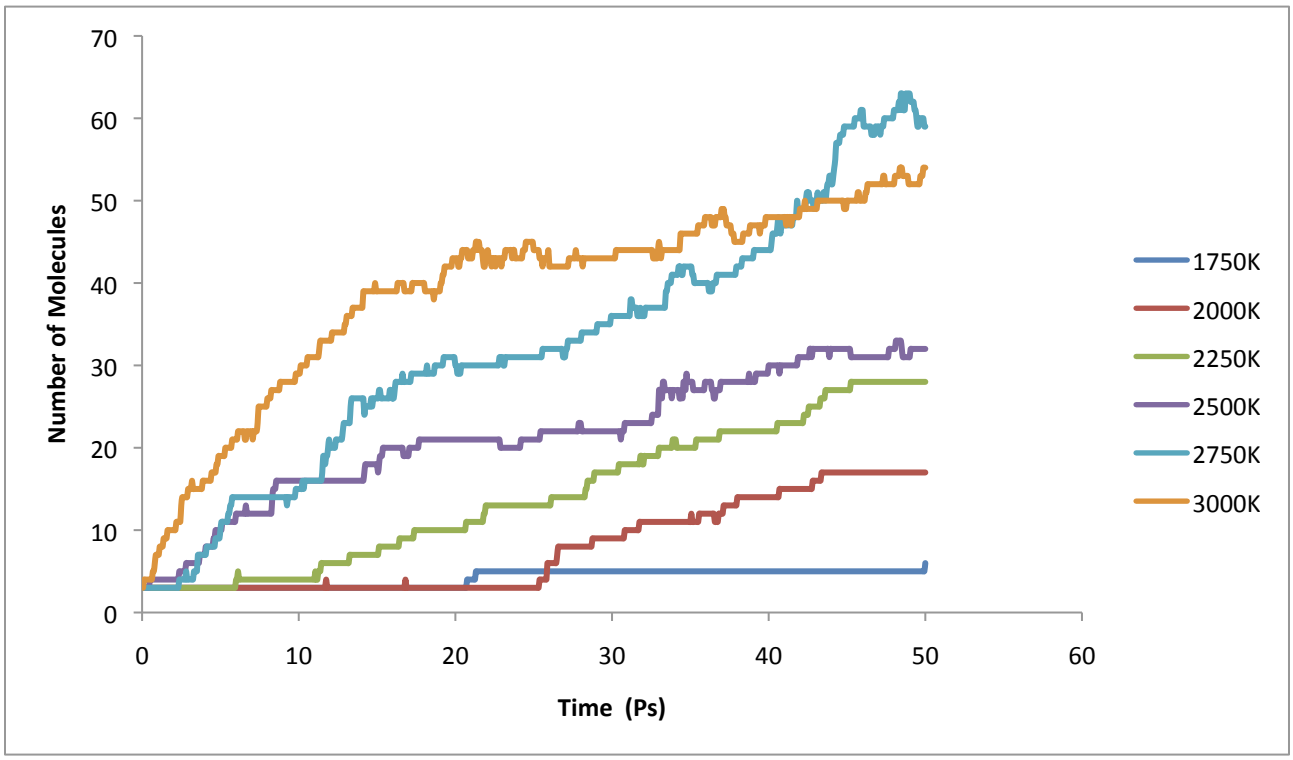

Figure 19: Results of NVT-MD simulation of inverted stack of three Campana asphaltene units at different temperatures.

The evolution of the molecular system as a function of the simulation time can also be followed. This evolution is shown in Figure 20 for the single Campana asphaltene unit NVT-MD simulation at 3000K where the starting atomic configuration and that after the 50 ps simulation are both depicted. The decomposition initiates with the breaking of the C-O bond between the aliphatic and the aromatic part of the molecule; the oxygen stays with the aliphatic part of the molecule. This event is similar at all the temperatures that were studied. As the simulation proceeds, the aliphatic part undergoes further decomposition to species of smaller molecular mass. However, the exact way it decomposes is different at different temperatures. At temperatures up to 2500K, the aromatic part of the molecule remains stable during the entire simulation, whereas at higher temperatures, the aromatic part also undergoes decomposition to produce smaller fragments with lower molecular mass. In the case of the stacks, the decomposition pathways are similar to those of the single Campana unit, with the aromatic unit remaining intact at lower temperatures and shorter time scales. The molecular formula of the products obtained from MD-NVT simulations of a single Campana molecule and its parallel, anti-parallel, and inverted stacks at 3000K are presented in Table 3.

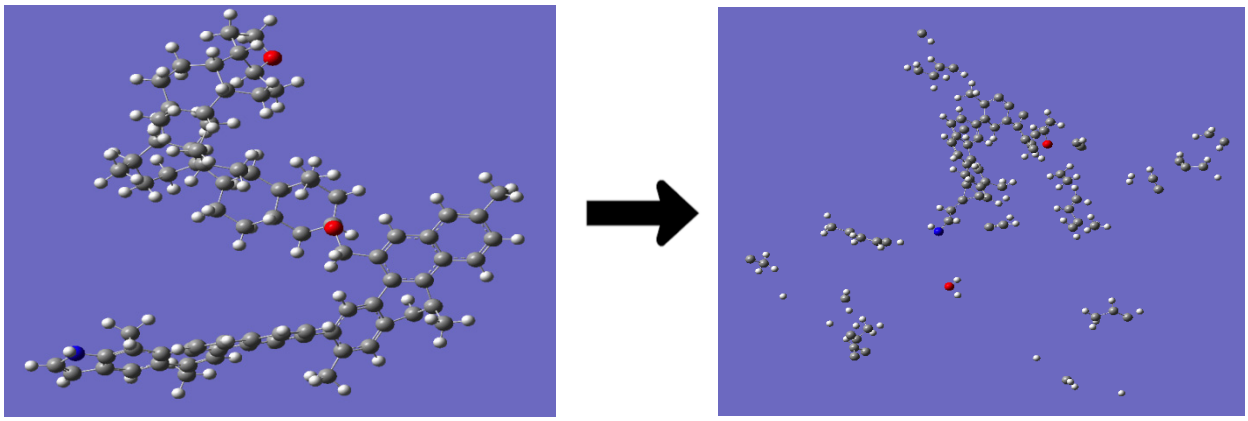

Figure 20: Optimized Campana asphaltene (left), which was the starting point for the ReaxFF MD simulation, and fragments after ReaxFF pyrolysis simulation (right).

Table 3: Molecular evolution from MD-NVT simulation of single Campana asphaltene unit, along with that for the three different stacks that were studied

Single Campana	Parallel Stack	Anti-parallel Stack	Inverted Stack
C41H27	3C2H4	3C3H5	C8H11
C5H5	5C2H3	2C4H7	C2HO
C2H5	C7H9O	5C2H3	4C2H4
HN	8C2H2	C4H5	2C2H
O	3C3H4	2CO	5C2H2
C	2C3H3	2C5H7	C2H3
2C3H3	6CH3	C3H6	4CH3
5C2H3	C38H31O	4C2H4	C4H5
CH3	6C2H	17C2H	2C6H9
C2H2	C32H20	C6H9	2C3H3
C5H9	C3	CH2O	4CH2O
C3H4	C2H2N	3CH3	3CH4
C2H	C3H5N	9C2H2	C41H30N
CH2O	CH3O	C3H4	C42H28N
7H	2C4H2	C2HO	C7H11
2H2	12H2	2C3H3	C42H27N
	C4H7	4C2	4C4H6
	H	C3H	9H2
	C7H12	3CH2	C3H2
	C8H10	C7H5	H
	CH4O	C4H6	C5H8
	H2O	C3H2N	CO
	C41H30	C6H10	2C5H7
	H2N	6H2	C3H6
	C4H6	C9H5	
	C2H2O	C22H18N	
	C2	2C6H7	
	C3H6	C7H8O	
	C6H8	C4H2	
		C4H3	
		CN	
		H	
		C2H5	
		C13H22	
		C2H2O	

VIII: Summary and Future Research

Starting with existing literature 2D atomic structures, 3D models have been established for both a Green River kerogen and for a set of six asphaltene structures. The development of these 3D models has allowed for the subsequent calculation of (1) a number of observables, namely ^{13}C NMR chemical shifts, vibrational frequencies, and PDF curves, (2) asphaltene stacking and (3) the interaction between the organic and inorganic components for asphaltenes.

These calculations have demonstrated:

1. The ability of modern computational chemistry tools to establish 3D atomic scale models of complex materials and large systems such as kerogen.
2. The feasibility of calculating observables such as ^{13}C NMR chemical shifts, vibrational frequencies, and PDF curves from these models.
3. The sensitivity of some of these observables (^{13}C NMR chemical shifts, vibrational frequencies) to structural differences between models.
4. The ability to simulate the pyrolysis process to gain information on the product distribution using these models.

Unfortunately, for this report there was limited experimental data with which to compare theoretical results. However, experimental data will soon be available with the recent (May 2010) acquisition of the Skyline 16 oil shale core from the Green River Formation in the Uinta Basin. Participants on the Oil Sands/Oil Shale project have identified three initial one-foot sections of interest from which to take samples. These three regions include two from the organic-rich R-7 or Mahogany Zone (one at the peak richness and one at a slightly leaner point) and a third from the upper R-6, which has an organic content similar to the leaner of the two Mahogany Zone samples. Studies are underway on the shale from these regions and the kerogen is currently being isolated from the shale. For oil sands, several potential asphaltenes sources have been discussed, but nothing has yet been selected.

In addition, arrangements have been made to obtain both SAXS and PDF data at the Advanced Photon Source at Argonne National Laboratory. The first visit to APS/ANL is scheduled for the last week of March 2011. During this visit, SAXS and hopefully PDF data will be obtained on both the raw oil shale and on the isolated kerogen. Once the isolated kerogen is obtained from each of these regions, ^{13}C NMR spectra and IR spectra will be measured at the University of Utah. Subsequent to the identification of appropriate asphaltene samples, similar measurements will be performed on those samples.

Specific future goals include:

1. Continued work on asphaltene stacking and interaction with the inorganic matrix. Specifically, the lack of binding measured in the calculations completed to date for both asphaltene stacking and asphaltene-illite interactions needs to be further explored to determine if this is possibly due to insufficiencies in the level of theory used. In addition, the mineralogical analyses being performed on the Skyline 16 core will provide valuable information on other inorganic substrates to use in the modeling.
2. Continued exploration on the best theory possible in the calculations, especially those used in the ^{13}C NMR chemical shift data and IR vibrational frequencies. It is well known that larger basis sets provide more reliable values for both of these calculations; however, the size of basis set that is feasible is limited by the large size of these systems, especially that of the kerogen model.
3. Once more experimental data is obtained on the oil shale and kerogen isolated from the shale, the agreement between the experimental data and that calculated using the developed model can be better evaluated. This comparison will guide adjustments to the model. For instance, some early ^{13}C NMR data supports a model with aromatic clusters connected by aliphatic chains containing about twelve carbons with little branching.
4. Expansion of the pyrolysis modeling to include simulations on the kerogen model, on multiple asphaltene units, and on the models that include the inorganic substrate. These results can then be compared to the product distribution obtained from the experimental pyrolysis of both the oil shale and the isolated kerogen.
5. Extension of the kerogen modeling to other types/sources of kerogen (e.g., kurkersite), possibly using existing literature data on these materials.

IX: References

[1] a) Durand, B; Vanderbroucke, M. As cited in *Kerogen, Insoluble Organic Matter From Rocks*, B. Durand, ed., Technip, **1980**, p. 218 and 319. b) Lille, U.; Heinmaa, I.; Pehk, T. *Fuel* **2003**, *82*, 799. c) Faulon, J.L.; Vandernbroucke, M.; Drappier, J.M.; Behar, F.; Romero, M. *Organic Geochemistry* **1990**, *6*, 981. d) Faulon, J.L. *Prediction, elucidation et modelisation moleculaire: algorithms et applications*. **1991,** Ph. D. Thesis, as cited in *Oil & Gas Science and Technology – Rev. IFP*, **2003**, *58*, 243-269.

[2] Siskin, M.; Scouten, C.G.; Rose, K.D.; Aczel, T.; Colgrove, S.G.; Pabst, R.E., Jr., in *Composition, Geochemistry and Conversion of Oil Shales*, NATO ASI Series C, Vol 455, Ed. Snape, C., Kluwer Academic Publishers, Boston, 1995

[3] a) Groenzin, H.; Mullins, O.C. *Energy & Fuels*, **2000**, *14*, 677-684. b) Gray, M.R. *Energy & Fuels*, **2003**, *17*, 1566-1569. c) Sheremata, J.M.; Gray, M.R.; Dettman, H.D.; McCaffrey, W.C. *Energy & Fuels*, **2004**, *18*, 1377-1384.

[4] Siskin, M.; Kelemen, S.R.; Eppig, C.P.; Brown, L.D.; Afeworki, M. *Energy & Fuels*, **2006**, *20*, 1227-1234.

[5] HyperChem(TM) Professional 7, Hypercube, Inc., 1115 NW 4th Street, Gainesville, Florida 32601, USA.

[6] Schmidt, M.W.; Baldridge, K.K.; Boatz,J.A.; Elbert, S.T.; Gordon, M.S.; Jensen, J.J.; Koseki, S.; Matsunaga, N.; Nguyen, K.A.; Su, S.; Windus, T.L.; Dupuis, M.; Montgomery, J.A. *J. Comput. Chem.* **1993**, *14*, 1347.

[7] Gaussian 09, Revision A.1, Frisch, M.J.; Trucks, G.W.; Schlegel, H.B.; Scuseria, G.E.; Robb, M.A.; Cheeseman, J.R.; Scalmani, G.; Barone, V.; Mennucci, B.; Petersson, G.A.; Nakatsuji, H.; Caricato, M.; Li, X.; Hratchian, H.P.; Izmaylov, A.F.; Bloino, J.; Zheng, G.; Sonnenberg, J.L.; Hada, M.; Ehara, M.; Toyota, K.; Fukuda, R.; Hasegawa, J.; Ishida, M.; Nakajima, T.; Honda, Y.; Kitao, O.; Nakai, H.; Vreven, T.; Montgomery, Jr., J. A.; Peralta, J.E.; Ogliaro, F.; Bearpark, M.; Heyd, J.J.; Brothers, E.; Kudin, K.N.; Staroverov, V.N.; Kobayashi, R.; Normand, J.; Raghavachari, K.; Rendell, A.; Burant, J.C.; Iyengar, S.S.; Tomasi, J.; Cossi, M.; Rega, N.; Millam, N.J.; Klene, M.; Knox, J.E.; Cross, J.B.; Bakken, V.; Adamo, C.; Jaramillo, J.; Gomperts, R.; Stratmann, R.E.; Yazyev, O.; Austin, A.J.; Cammi, R.; Pomelli, C.; Ochterski, J.W.; Martin, R.L.; Morokuma, K.; Zakrzewski, V.G.; Voth, G.A.; Salvador, P.; Dannenberg, J.J.; Dapprich, S.; Daniels, A.D.; Farkas, Ö.; Foresman, J.B.; Ortiz, J.V.; Cioslowski, J.; Fox, D.J. Gaussian, Inc., Wallingford CT, 2009.

[8] a) van Duin, A.C.T.; Dasgupta, S.; Lorant, F.; Goddard III, W.A. *J. Phys. Chem. A* **2001***, 105,* 9396-9409.
b) Chenoweth, K.; van Duin, A.C.T.; Goddard III, W.A. *J. Phys. Chem. A* **2008**, *112*, 1040–1053.

[9] Proffen, T.; Neder, R.B. *J. Appl. Crystallogr.* **1997**, *30*, 171.

[10] Allinger, N.L. *J. Am. Chem. Soc.*, **1977**, *99*, 8127.

[11] a) Dickie, J.P.; Yen, T.F. *Anal. Chem.* **1967**, *39*, 1847-1852. b) Yen, T.F.; Erdman, J.G.; Pollack, S.S. *Anal. Chem.* **1961**, *33*, 1587-1594. c) Brandt, H.C.A.; Hendriks, E.M.; Michels, M.A.J.; Visser, F. *J. Phys. Chem.* **1995**, *99*, 10430-10432. d) Tanaka, R.; Hunt, J.E.; Winans, R.E.; Thiyagarajan, P.; Sato, S,; Takanohashi, T. *Energy & Fuels*, **2003**, *17*, 127-134. e) Mostowfi, F.; Indo, K.; Mullins, O.C.; McFarlane, R. *Energy & Fuels*, **2009**, *23*, 1194-1200.

[12] Zhao, G.; Truhlar, D.G. *Theor. Chem. Acc.* **2008**, *120*, 215-241.

[13] Boys, S.F.; Bernardi, F. *Mol. Phys.* **1970**, *19*, 553.

[14] Drits, V.A.; Zviagina, B.B.; McCarty, D. K.; Salyn, A.L., *Am. Mineralogist* **2010**, *95*, 348. Used the RM30 coordinates with M=Al and T=Si.

[15] Rappe, A.K.; Casewit, C.J.; Colwell, K.S.; Goddard III, W.A. *J. Am. Chem. Soc.* **1992**, *114*, 10024-10035.

[16] Svergun, D.; Barberato, C.; Koch, M.H.J. *J. Appl. Crystallogr.* **1995**, *28*, 768-773.

[17] Tjioe, E.; Heller, W.T. *J. Appl. Crystallogr.* **2007**, *40*, 782-785.

[18] Jameson, C.J.; Jameson, A.K. *Chem. Phys. Lett.* **1987**, *134*, 461.

[19] Chenoweth, K.; Cheung, S.; van Duin, A.C.T.; Goddard III, W. A.; Kober, E.M. *J. Am. Chem. Soc.* **2005**, *127*, 7192-7202.

[20] Zhang, L.; Zybin, S.V.; van Duin, A.C.T.; Dasgupta, S.; Goddard III, W. A.; Kober, E.M. *J. Phys. Chem. A* **2009**, *113*, 10619-10640.

[21] Chenoweth, K.; van Duin, A.C.T.; Dasgupta, S.; Goddard III, W. A. *J. Phys. Chem. A* **2009**, *113*, 1740-1746.

[22] Mueller, J.E.; van Duin, A.C.T.; Goddard III, W. A. *J. Phys. Chem. C* **2010**, *114*, 5675-5685.

[23] Salmon, E.; van Duin, A.C.T.; Lorant, F.; Marquaire, P.-M.; Goddard III, W. A. *Org. Geochem.* **2009**, *40*, 416-427.

[24] Salmon, E.; van Duin, A.C.T.; Lorant, F.; Marquaire, P.-M.; Goddard III, W. A. *Org. Geochem.* **2009**, *40*, 1195-1209.

[25] Evans, D.J.; Holian, B.L. *J. Chem. Phys.* **1985**, *83*, 4069-4074.

[26] Berendsen, H.J.C.; Postma, J.P.M.; van Gunsteren, W.F.; DiNola, A.; Haak, J.R. *J. Chem. Phys.* **1984**, *81*, 3684-3690.

[27] Adelman, S.A.; Doll, J.D. *J. Chem. Phys.* **1976**, *64*, 2375-2388.

National Energy Technology Laboratory

626 Cochrans Mill Road
P.O. Box 10940
Pittsburgh, PA 15236-0940

3610 Collins Ferry Road
P.O. Box 880
Morgantown, WV 26507-0880

13131 Dairy Ashford, Suite 225
Sugarland, TX 77478

1450 Queen Avenue SW
Albany, OR 97321-2198

2175 University Ave. South
Suite 201
Fairbanks, AK 99709

Visit the NETL website at:
www.netl.doe.gov

Customer Service:
1-800-553-7681